
1 **Underestimation of Anthropogenic Organosulfates in Atmospheric**
2 **Aerosols in Urban Regions**

3 *Yanting Qiu^{1#}, Junrui Wang^{1#}, Tao Qiu², Jiajie Li³, Yanxin Bai⁴, Teng Liu¹, Ruiqi Man¹,*
4 *Taomou Zong¹, Wenxu Fang¹, Jiawei Yang¹, Yu Xie¹, Zeyu Feng¹, Chenhui Li³, Ying Wei³,*
5 *Kai Bi⁵, Dapeng Liang², Ziqi Gao⁶, Zhijun Wu^{1,7,*}, Yuchen Wang^{4,*}, Min Hu¹*

6 ¹ State Key Laboratory of Regional Environment and Sustainability, International Joint
7 Research Center for Atmospheric Research (IJRC), College of Environmental Sciences
8 and Engineering, Peking University, Beijing, China

9 ² Key Lab of Groundwater Resources and Environment of the Ministry of Education,
10 College of New Energy and Environment, Jilin University, Changchun, China

11 ³ College of Environment and Ecology, Laboratory of Compound Air Pollutions
12 Identification and Control, Taiyuan University of Technology, Taiyuan, China

13 ⁴ College of Environmental Science and Engineering, Hunan University, Changsha,
14 China

15 ⁵ Beijing Weather Modification Center, Beijing Meteorological Service, Beijing, China

16 ⁶ University of Virginia Environmental Institute, Charlottesville, United States

17 ⁷ Collaborative Innovation Center of Atmospheric Environment and Equipment
18 Technology, Nanjing University of Information Science and Technology, Nanjing, China

19 #: Yanting Qiu and Junrui Wang contributed equally to this work

20 *Correspondence Author:

21 Zhijun Wu (zhijunwu@pku.edu.cn) and Yuchen Wang (ywang@hnu.edu.cn)

23 **ABSTRACT**

24 Organosulfates (OSs) are important components of organic aerosols, which serve as
25 critical tracers of secondary organic aerosols (SOA). However, molecular composition,
26 the relationship between OSs and their precursors, and formation driving factors of OSs
27 at different atmospheric conditions have not been fully constrained. In this work, we
28 integrated OS molecular composition, precursor-constrained positive matrix factorization
29 (PMF) source apportionment, and OS-precursor correlation analysis to classify OS
30 detected from PM_{2.5} samples according to their volatile organic compounds (VOCs)
31 precursors collected from three different cities (Beijing, Taiyuan, and Changsha) in China.
32 This new approach enables the accurate classification of OSs from molecular perspective.
33 Compared with conventional classification methods, we found the mass fraction of
34 Aliphatic OSs (including nitrooxy OSs; NOSs) increased by 22.0%, 17.8%, and 10.3%
35 in Beijing, Taiyuan, and Changsha, respectively, highlighting the underestimation of
36 Aliphatic OSs in urban regions. The formation driving factors of Aliphatic OSs during
37 the field campaign were further investigated. We found that elevated aerosol liquid water
38 content promoted the formation of Aliphatic OSs only when aerosols transition from non-
39 liquid state to liquid state. In addition, enhanced inorganic sulfate mass concentrations,
40 and O_x (O_x = NO₂ + O₃) concentrations, as well as decreased aerosol pH commonly
41 facilitated the formation of Aliphatic OSs. These results reveal a significant
42 underestimation of OSs derived from anthropogenic emissions in wintertime, particularly
43 Aliphatic OSs, highlighting the need for a deeper understanding of SOA formation and
44 composition in urban environments.

45 **KEY WORDS:** organosulfate; non-target analysis; high-resolution mass spectrometry;
46 secondary organic aerosol; PMF source apportionment

48 1. Introduction

49 Due to the diversity of natural and anthropogenic emissions and the complexity of atmospheric
50 chemistry, investigating the chemical characterization and formation mechanisms of secondary
51 organic aerosols (SOA) remains challenging. Among SOA components, organosulfates (OSs) have
52 emerged as key tracers (Brüggemann et al., 2020; Hoyle et al., 2011), as their formation is primarily
53 governed by secondary atmospheric processes. Moreover, OS significantly influence the aerosol
54 physicochemical properties, including acidity (Riva et al., 2019; Zhang et al., 2019), hygroscopicity
55 (Estillore et al., 2016; Ohno et al., 2022; Hansen et al., 2015), and light-absorption properties (Fleming
56 et al., 2019; Jiang et al., 2025). Therefore, a deeper understanding of OS abundance, sources, and
57 formation drivers is crucial for elucidating SOA formation and its properties.

58 Quantifying OS abundance is critical to assess their contribution to SOA. However, this is
59 difficult due to the large number and structural diversity of OSs molecules and the lack of authentic
60 standards. Most studies quantify a few representative OSs using synthetic or surrogate standards
61 (Wang et al., 2020; Wang et al., 2017; Huang et al., 2018b; He et al., 2022), while non-target analysis
62 (NTA) with high-resolution mass spectrometry (HRMS) offers broader molecular characterization
63 (Huang et al., 2023a; Wang et al., 2022b; Cai et al., 2020). Although NTA combined with surrogate
64 standards allows molecular-level (semi-)quantification, overall OS mass concentration remain
65 underestimated, and many OSs remain unidentified (Lukács et al., 2009; Cao et al., 2017; Tolocka and
66 Turpin, 2012; Ma et al., 2025).

67 Classifying OS based on their precursors is a powerful approach for understanding OS formation
68 from a mechanistic perspective. OSs from specific precursors generally share similar elemental
69 compositions, with characteristic ranges of C atoms, double bond equivalents (DBE), and aromaticity
70 equivalents (Xc). For example, isoprene-derived OSs typically contain 4–5 C atoms; monoterpene-
71 and sesquiterpene-derived OSs usually have 9–10 and 14–15 C atoms, respectively (Lin et al., 2012;
72 Riva et al., 2016c; Wang et al., 2019a; Surratt et al., 2008; Riva et al., 2015). An “OS precursor map,”
73 correlating molecular weight and carbon number based on chamber studies, has been developed to
74 classify OSs accordingly (Wang et al., 2019a). However, these approaches often oversimplify OS
75 formation by relying solely on elemental composition, leaving many OSs without identified precursors.

76 The formation mechanisms of OS remain incompletely understood, though several driving
77 factors have been identified through controlled chamber experiments and ambient observations. For
78 instance, increased aerosol liquid water content (ALWC) enhances OS formation by promoting the
79 uptake of gaseous precursors (Xu et al., 2021a; Wang et al., 2021b). Inorganic sulfate can also affect
80 OS formation by acting as nucleophiles via epoxide pathway (Eddingsaas et al., 2010; Wang et al.,
81 2020). However, meteorological conditions vary across cities, meaning the relative importance of
82 these factors may differ by location. Thus, evaluating these formation drivers under diverse
83 atmospheric conditions is essential. Identifying both common and region-specific drivers is key to a
84 comprehensive understanding of OS formation mechanisms.

85 In this study, we employed NTA using ultra-high performance liquid chromatography (UHPLC)
86 coupled with high-resolution mass spectrometry (HRMS) to characterize OS molecular composition
87 in PM_{2.5} samples from three cities. Identified OSs were classified by their VOCs precursors, including

88 aromatic, aliphatic, monoterpene, and sesquiterpene VOCs, via precursor-constrained positive matrix
89 factorization (PMF). Mass concentrations were quantified or semi-quantified using authentic or
90 surrogate standards. Additionally, spatial variations in OS mass concentrations and environmental
91 conditions were analyzed to distinguish both common and site-specific drivers of OS formation.

92 **2. Methodology**

93 **2.1 Sampling and Filter Extraction**

94 Field observations were conducted during winter (December 2023 to January 2024) at three urban
95 sites in China: Beijing, Taiyuan, and Changsha. The site selection was based on contrasts in winter
96 meteorological conditions and dominate $\text{PM}_{2.5}$ sources. For meteorological conditions, Beijing and
97 Taiyuan represent northern Chinese cities with cold, dry conditions (low RH). In comparison,
98 Changsha is characterized by relatively higher winter RH. In terms of $\text{PM}_{2.5}$ sources, Taiyuan is a
99 traditional industrial and coal-mining base, Changsha's pollution profile is more influenced by traffic
100 and domestic cooking emissions, whereas Beijing is characterized by a high mass fraction of
101 secondary aerosols. This enables a comparative analysis of OS formation mechanisms under varied
102 atmospheric conditions. In Beijing, $\text{PM}_{2.5}$ samples were collected at the Peking University Atmosphere
103 Environment Monitoring Station (PKUERS; 40.00°N, 116.32°E), as detailed in previous studies
104 (Wang et al., 2023a). Sampling in Taiyuan and Changsha took place on rooftops at the Taoyuan
105 National Control Station for Ambient Air Quality (37.88°N, 112.55°E) and the Hunan Hybrid Rice
106 Research Center (28.20°N, 113.09°E), respectively (see Figure S1).

107 Daily $\text{PM}_{2.5}$ samples were collected on quartz fiber filters ($\phi = 47$ mm, Whatman Inc.) from 9:00
108 to 8:00 local time the next day. All quartz fiber filters were pre-baked at 550 °C for 9 hours before
109 sampling to remove the background organic matters. In Beijing and Taiyuan, RH-resolved sampling
110 was performed using a home-made RH-resolved sampler, stratifying daily samples into low (RH \leq
111 40%), moderate (40% $<$ RH \leq 60%), and high (RH $>$ 60%) RH regimes with the sampling flow rate
112 of 38 L/min. Due to persistently high RH in Changsha, a four-channel sampler (TH-16, Wuhan
113 Tianhong Inc.) collected $\text{PM}_{2.5}$ samples without RH stratification with the flow rate of 16.7 L/min.
114 Consequently, Beijing and Taiyuan collected one or more samples daily, whereas Changsha collected
115 one sample per day. A total of 40, 64, and 30 samples were obtained from Beijing, Taiyuan, and
116 Changsha, respectively. The samples were stored in a freezer at -18 °C immediately after collection.
117 The maximum duration between the completion of sampling and the start of chemical analysis was
118 approximately 40 days. Prior to analysis, all samples were equilibrated for 24 hours under controlled
119 temperature (20 \pm 1 °C) and RH (40-45%) within a clean bench, in order to allow the filters to reach
120 a stable, reproducible condition for subsequent handling and to minimize moisture condensation.
121 Average daily $\text{PM}_{2.5}$ mass concentrations and RH during sampling are summarized in Table S1.

122 Sample extraction followed established protocols (Wang et al., 2020). Briefly, filters were
123 ultrasonically extracted twice for 20 minutes. A total volume of 10 mL of LC-MS grade methanol
124 (Merck Inc.) was used for each sample. All extracts were filtered through 0.22 μm PTFE syringe filters,
125 and evaporated under a gentle stream of high-purity N_2 ($>99.99\%$). The dried extracts were then
126 redissolved in 2 mL of LC-MS grade methanol for analysis. This step was necessary to achieve

127 sufficient sensitivity for the detection of OSs with low concentration.

128 During the campaign, gaseous pollutants (SO_2 , NO_2 , O_3 , CO) were monitored using automatic
129 analyzers. $\text{PM}_{2.5}$ and PM_{10} mass concentrations were measured by tapered element oscillating
130 microbalance (TEOM). Water-soluble ions (Na^+ , NH_4^+ , K^+ , Mg^{2+} , Ca^{2+} , Cl^- , NO_3^- , SO_4^{2-}) were
131 analyzed with the Monitor for AeRosols and Gases in ambient Air (MARGA) coupled with ion
132 chromatography. Organic carbon (OC) and elemental carbon (EC) were quantified by online OC/EC
133 analyzers or carbon aerosol speciation systems. Trace elements in $\text{PM}_{2.5}$ were determined by X-ray
134 fluorescence spectrometry (XRF). Additionally, VOCs concentrations were measured using an online
135 gas chromatography-mass spectrometry (GC-MS) system with a one-hour time resolution in Taiyuan
136 and Changsha. Table S2 summarizes the monitoring instruments deployed at each site. All instruments
137 were calibrated to ensure the reliability of the measurement data. Specifically, the online gas pollutants
138 and particulate matter automatic analyzers underwent automatic zero/span checks every 24 hours at
139 0:00 local time. For MARGA-ion chromatography, OC/EC analyzers, and XRF systems were
140 calibrated weekly. The online GC-MS system was automatically calibrated every 24 hours using
141 standard VOCs mixture.

142 2.2 Identification of Organosulfates

143 The molecular composition of $\text{PM}_{2.5}$ extracts was analyzed using an ultra-high performance
144 liquid chromatography (UHPLC) system (Thermo Ultimate 3000, Thermo Scientific) coupled with an
145 Orbitrap HRMS (Orbitrap Fusion, Thermo Scientific) equipped with an electrospray ionization (ESI)
146 source operating in negative mode. Chromatographic separation was achieved on a reversed-phase
147 Accucore C18 column (150 × 2.1 mm, 2.6 μm particle size, Thermo Scientific). For tandem MS
148 acquisition, full MS scans (m/z 70–700) were collected at a resolving power of 120,000, followed by
149 data-dependent MS/MS (ddMS²) scans (m/z 50–500) at 30,000 resolving power. Detailed UHPLC-
150 HRMS² parameters are provided in Text S1.

151 NTA was performed using Compound Discoverer (CD) software (version 3.3, Thermo Scientific)
152 to identify chromatographic peak features (workflow details in Table S3). Molecular formulas were
153 assigned based on elemental combinations $\text{C}_c\text{H}_h\text{O}_o\text{N}_n\text{S}_s$ ($c = 1\text{--}90$, $h = 1\text{--}200$, $o = 0\text{--}20$, $n = 0\text{--}1$, $s =$
154 $0\text{--}1$) within a mass tolerance of 0.005 Da with up to one ^{13}C isotope. Formulas with hydrogen-to-
155 carbon (H/C) ratios outside 0.3–3.0 and oxygen-to-carbon (O/C) ratios beyond 0–3.0 were excluded
156 to remove implausible assignments. We calculated the double bond equivalent (DBE) and aromatic
157 index represented by X_c based on assigned elemental combinations using eqs. (1) and (2), where m
158 and k were the fractions of oxygen and sulfur atoms in the π -bond structures of a compound (both m
159 and k were presumed to be 0.50 in this work (Yassine et al., 2014)).

$$160 \quad \text{DBE} = c - 0.5h + 0.5n + 1 \quad (1)$$

$$161 \quad X_c = (3 \times (\text{DBE} - m \times o - k \times s) - 2) / (\text{DBE} - m \times o - k \times s) \quad (\text{if } \text{DBE} < (m \times o + \\ 162 \quad k \times s) \text{ or } X_c < 0, \text{ then } X_c \text{ was set to } 0) \quad (2)$$

163 In eq. (2), X_c is an important indicator of whether aromatic rings exist in a molecule. Studies
164 have proved that a molecule is considered aromatic if its X_c value exceeds 2.50 (Ma et al., 2022;
165 Yassine et al., 2014). OSs were selected based on compounds with $\text{O/S} \geq 4$ and HSO_4^- (m/z 96.96010)
166 fragments were observed in their corresponding MS² spectra. Among them, if N number is 1, $\text{O/S} \geq 7$,

167 and their MS^2 spectra showed ONO_2^- (m/z 61.98837) fragment, these OSs were defined as nitrooxy
168 OSs (NOSs). It should be noted that several CHOS (composed of C, H, O, and S atoms, hereinafter)
169 and CHONS species were not determined as OSs due to their low-abundance and insufficient to trigger
170 reliable data-dependent MS^2 acquisition, which may lead to an underestimation of total OS mass
171 concentration.

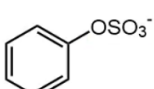
172 **2.3 Classification and Quantification/Semi-quantification of Organosulfates**

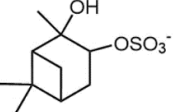
173 To ensure the reliability of quantitative analysis and source attribution, this study focuses on OS
174 species with $\text{C} \geq 8$. The exclusion of smaller OSs ($\text{C} \leq 7$) is based on challenges in their unambiguous
175 identification, including co-elution with interfering compounds (Liu et al., 2024), and higher
176 uncertainty in precursor assignment due to the lack of characteristic “tracer” molecules in laboratory
177 experiments. Though re-dissolve using pure methanol may not be the ideal solvent for retaining polar,
178 early-eluting compounds on the reversed-phase column, it provided a consistent solvent for the
179 analysis of the mid- and non-polar OS species ($\text{C} \geq 8$) that are the focus of this study.

180 To classify the identified OSs, we employed and compared two distinct classification approaches.
181 Firstly, a conventional classification approach relies primarily on precursor–product relationships
182 established through controlled laboratory chamber experiments and field campaigns (Zhao et al., 2018;
183 Wang et al., 2021a; Deng et al., 2021; Xu et al., 2021b; Mutzel et al., 2015; Brüggemann et al., 2020;
184 Yang et al., 2024; Duporté et al., 2020; Huang et al., 2023b; Wang et al., 2022b; Riva et al., 2016a).
185 Based on these established precursor–product relationships, detected OSs and NOSs were classified
186 into four groups: Monoterpene OSs (including Monoterpene NOSs, hereinafter), Aliphatic OSs
187 (including Aliphatic NOSs, hereinafter), Aromatic OSs (including Aromatic NOSs, hereinafter), and
188 Sesquiterpene OSs (including Sesquiterpene NOSs, hereinafter) (see Table S4 for details). It is
189 apparently that this approach has notable limitations when applied to detected OS in atmospheric
190 aerosols. A substantial fraction of detected OSs does not match known laboratory tracers and are thus
191 labeled Unknown OSs (including Unknown NOSs, hereinafter).

192 Synthetic α -pinene OSs ($\text{C}_{10}\text{H}_{17}\text{O}_5\text{S}^-$) and NOSs ($\text{C}_{10}\text{H}_{16}\text{NO}_7\text{S}^-$) served for (semi-)quantifying
193 Monoterpene and Sesquiterpene OSs. Their detailed synthesis procedure was described in previous
194 study (Wang et al., 2019b). Potassium phenyl sulfate ($\text{C}_6\text{H}_5\text{O}_4\text{S}^-$) and sodium octyl sulfate ($\text{C}_8\text{H}_{17}\text{O}_4\text{S}^-$)
195 were used for Aromatic OSs and Aliphatic OSs due to lack of authentic standards (Yang et al., 2023;
196 He et al., 2022; Staudt et al., 2014). Unknown OSs were semi-quantified by surrogates with similar
197 retention times (RT) (Yang et al., 2023; Huang et al., 2023b). Table 1 lists the standards, retention
198 times, and quantified categories. Unknown OSs were absent between 2.00–5.00 min and after 13.60
199 min.

200 **Table 1** Chemical structure, UHPLC retention time, and quantified categories of standards used in
201 the quantification/semi-quantification of OSs and NOSs

Formula (M-H)	m/z ([M-H] $^-$)	Chemical structure	UHPLC RT (min)	Quantified OSs categories
$\text{C}_6\text{H}_5\text{O}_4\text{S}^-$	172.99140		0.92	Aromatic OSs, Unknown OSs (RT 0.50-2.00 min)

$C_8H_{17}O_4S^-$	209.08530		10.30	Aliphatic OSs, Unknown OSs (RT 10.00-13.60 min)
$C_{10}H_{17}O_5S^-$	249.08022		7.73	Monoterpene OSs, Sesquiterpene OSs, Unknown OSs (RT 5.00-10.00 min)
$C_{10}H_{16}NO_7S^-$	294.06530		9.26	Monoterpene NOSs and Sesquiterpene NOSs

202 This quantification approach introduces inherent uncertainty, as differences in molecular
 203 structure and functional groups between a surrogate and detected OSs have different ionization
 204 efficiency (Ma et al., 2025), which is a well-documented challenge in NTA of complex mixtures.
 205 However, this approach provides a consistent basis for comparing the relative abundance of OS in
 206 different cities and their formation driving factors. Hence, the mass concentration of detected OSs is
 207 still reliable in understanding their classification and formation driving factors.

208 To classify the Unknown OSs, we first calculated the X_c of each species. Those with $DBE > 2$ and
 209 $X_c > 2.50$ were designated as Aromatic OSs (Yassine et al., 2014). Subsequently, constrained positive
 210 matrix factorization (PMF) analysis was performed using EPA PMF 5.0. The input matrix comprised
 211 the mass concentrations of 60 unclassified OS species across all samples.

212 Figure S2 shows the source profiles of PMF model. Four factors were identified in this study.
 213 Specifically, Factor 1 is identified as Aliphatic OSs due to the dominant contributions from species
 214 like $C_{11}H_{22}O_5S$ and $C_{12}H_{24}O_5S$, which possess low DBE and are characteristic of long-chain alkane
 215 oxidation (Yang et al., 2024). This assignment is strongly supported by the co-variation of this factor
 216 with n-dodecane. Similarly, Factor 2 is classified as Aromatic OSs, highlighted by the significant
 217 contribution of $C_{10}H_{10}O_7S$ and $C_{11}H_{14}O_7S$, which have been proved as OSs derived from typical
 218 aromatic VOCs (Riva et al., 2015). In addition, the high contributions of benzene, toluene, and styrene
 219 in Factor 2 further suggests that this factor should be classified as Aromatic OSs. As for Factor 3 and
 220 Factor 4 is confirmed by the prominence of established Monoterpene OSs (Surratt et al., 2008; Iinuma
 221 et al., 2007) (e.g., $C_{10}H_{18}O_5S$, $C_{10}H_{17}NO_7S$) and Sesquiterpene OSs (Wang et al., 2022b) (e.g.,
 222 $C_{14}H_{28}O_6S$, $C_{15}H_{25}NO_7S$), respectively. Moreover, isoprene showed high contribution in both Factors
 223 3 and 4. As monoterpenes and sesquiterpenes cannot be detected by online GC-MS, considering that
 224 monoterpenes and sesquiterpenes mainly originate from biogenic sources and strongly correlate with
 225 isoprene (Guenther et al., 2006; Sakulyanontvittaya et al., 2008), therefore, isoprene is used as a
 226 surrogate marker as Monoterpene OSs and Sesquiterpene OSs. High contribution of isoprene in
 227 Factors 3 and 4 proved that these factors were respectively determined as Monoterpene OSs and
 228 Sesquiterpene OSs. Based on marker species, Unknown OSs were further categorized into
 229 Monoterpene, Aromatic, Aliphatic, and Sesquiterpene OSs.

230 The model was executed with 10 runs to ensure stability. The ratio of $Q_{\text{robust}}/Q_{\text{true}}$ for this solution
 231 was stabilized below 1.50, indicating a robust fit without over-factorization. Furthermore, the scaled
 232 residual matrix (see Figure S3), demonstrating that residuals are randomly distributed and
 233 predominantly within the acceptable range of -3 to 3. Correlation coefficients between classified OSs
 234 and corresponding VOCs (Monoterpene OSs vs. isoprene; Aromatic OSs vs. benzene; Aliphatic OSs

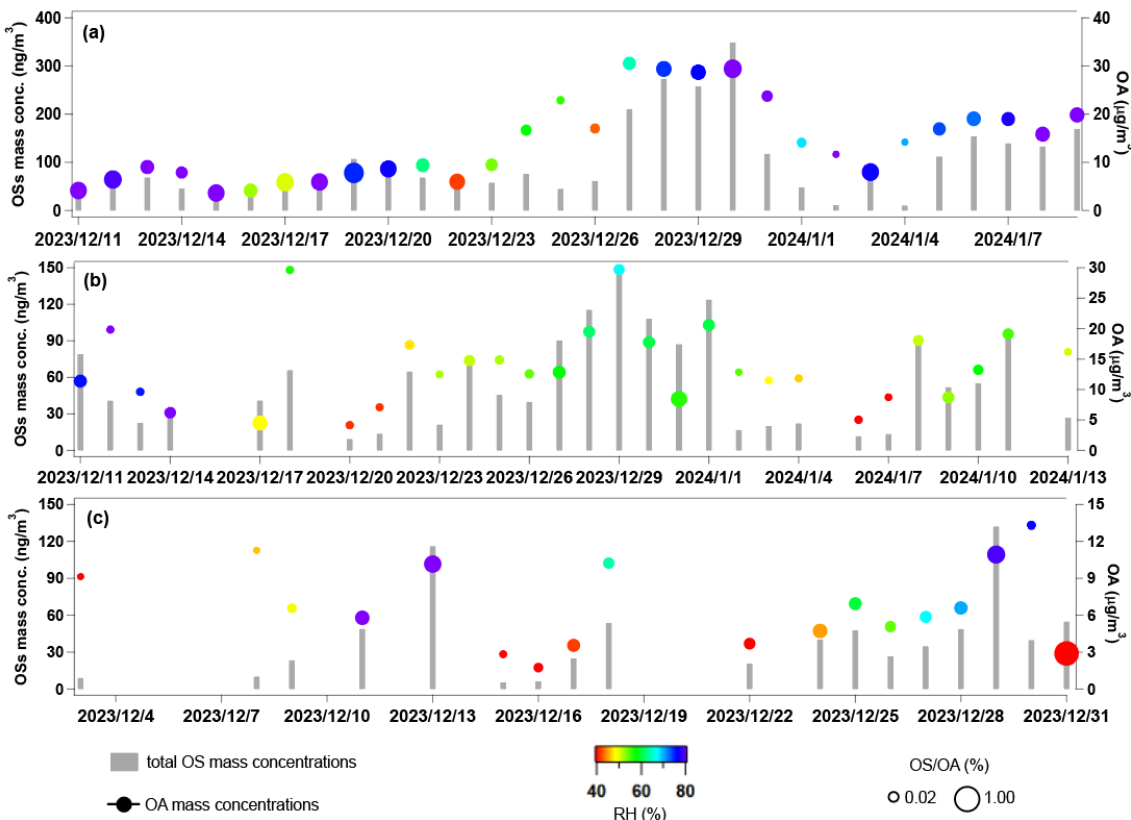
235 vs. n-dodecane; Sesquiterpene OSs vs. isoprene) were calculated as a statistical auxiliary variable to
236 verify the reliability of PMF results. The arithmetic mean of hourly VOCs within each corresponding
237 filter sampling period was calculated to align the time resolution of VOCs and OS mass concentration.
238 Species with $R < 0.40$ were excluded to avoid potential incorrect classification.

239 To validate classification accuracy, MS^2 fragment patterns were analyzed (Table S5). Diagnostic
240 fragments supported the assignments: Aliphatic OSs showed sequential alkyl chain cleavages ($\Delta m/z$
241 = 14.0157) and saturated alkyl fragments ($[C_nH_{2n+1}]^-$ or $[C_nH_{2n-1}]^-$); Monoterpene OSs displayed
242 $[C_nH_{2n-3}]^-$ fragments; Aromatic OSs exhibited characteristic aromatic substituent fragments ($[C_6H_5R-$
243 H] $^-$, R = alkyl, carbonyl, -OH, or H). While absolute certainty for every individual OS in a complex
244 ambient mixture is unattainable, integrating the precursor-constrained PMF model, tracer VOCs
245 correlation analysis, and MS^2 fragment patterns validation significantly reduces the likelihood of
246 systematic misclassification.

247 **3. Results and Discussion**

248 **3.1 Concentrations, Compositions, and Classification of Organosulfates**

249 Figure 1 shows the temporal variations of OS and organic aerosols (OA) mass concentrations, as
250 well as RH, during the sampling period across the three cities. The total mass concentration of OS
251 reported in this study is the sum of the (semi-)quantified concentrations of all individual OS species
252 that met the identification criteria described in Section 2.3. The mean OSs concentrations were (41.1
253 ± 34.5) ng/m 3 in Beijing, (57.4 ± 39.2) ng/m 3 in Taiyuan, and (102.1 ± 80.5) ng/m 3 in Changsha. Table
254 S6 summarizes the average concentrations of PM $_{2.5}$, OC, gaseous pollutants, OS mass concentrations,
255 and the mean meteorological parameters during sampling period for all three cities. OS accounted for
256 0.64% \pm 0.44%, 0.41% \pm 0.24%, and 0.76% \pm 0.34% of the total OA in Beijing, Taiyuan, and Changsha,
257 respectively.



258

259 **Figure 1** Temporal variations of daily total OS mass concentrations and average OA mass
 260 concentrations in (a) Changsha, (b) Taiyuan, and (c) Beijing. The markers of OA mass concentrations
 261 are colored by average RH during sampling period, and marker sizes indicate the OS/OA mass
 262 concentration ratios.

263 The highest OS mass concentrations and OS/OA ratios were observed in Changsha. As shown in
 264 Figure 1(a), a distinct episode with OS mass concentrations exceeding 300 ng/m^3 occurred between
 265 December 27th and 31st, leading to the elevated OS mass concentrations in Changsha. This episode
 266 coincided with a period of intense fireworks activity, as evidenced by significant increases in the
 267 concentrations of recognized fireworks tracers, especially Ba and K (see Figure S4), leading to an
 268 increase in SO_2 emission. We noted that though K may originate from biomass burning, its trend in
 269 concentration shows good consistency with that of Ba. Therefore, we still infer that fireworks activity
 270 are also the primary source of K. Considering persistently high RH (consistently $>70\%$) during this
 271 period, as displayed in Figure S5, ALWC ($117.9 \mu\text{g/m}^3$ in average) therefore increased and facilitated
 272 the heterogeneous oxidation of SO_2 to particulate sulfate (Wang et al., 2016a; Ye et al., 2023). Since
 273 particulate sulfate serves as a key reactant in OS formation pathways, its elevated concentration
 274 directly promoted OS production (Xu et al., 2024; Wang et al., 2020). Furthermore, fireworks activity
 275 led to concurrent increases in the concentrations of transition metals, notably Fe and Mn (Figure S4),
 276 which are known to catalyze aqueous-phase radical chemistry and OS formation (Huang et al., 2019;
 277 Huang et al., 2018a). Therefore, the pronounced OS mass concentration during this period is attributed
 278 to a combination of elevated precursor emissions (SO_2), high-RH conditions favoring aqueous-phase
 279 processing, and the potential catalytic role of co-emitted transition metals.

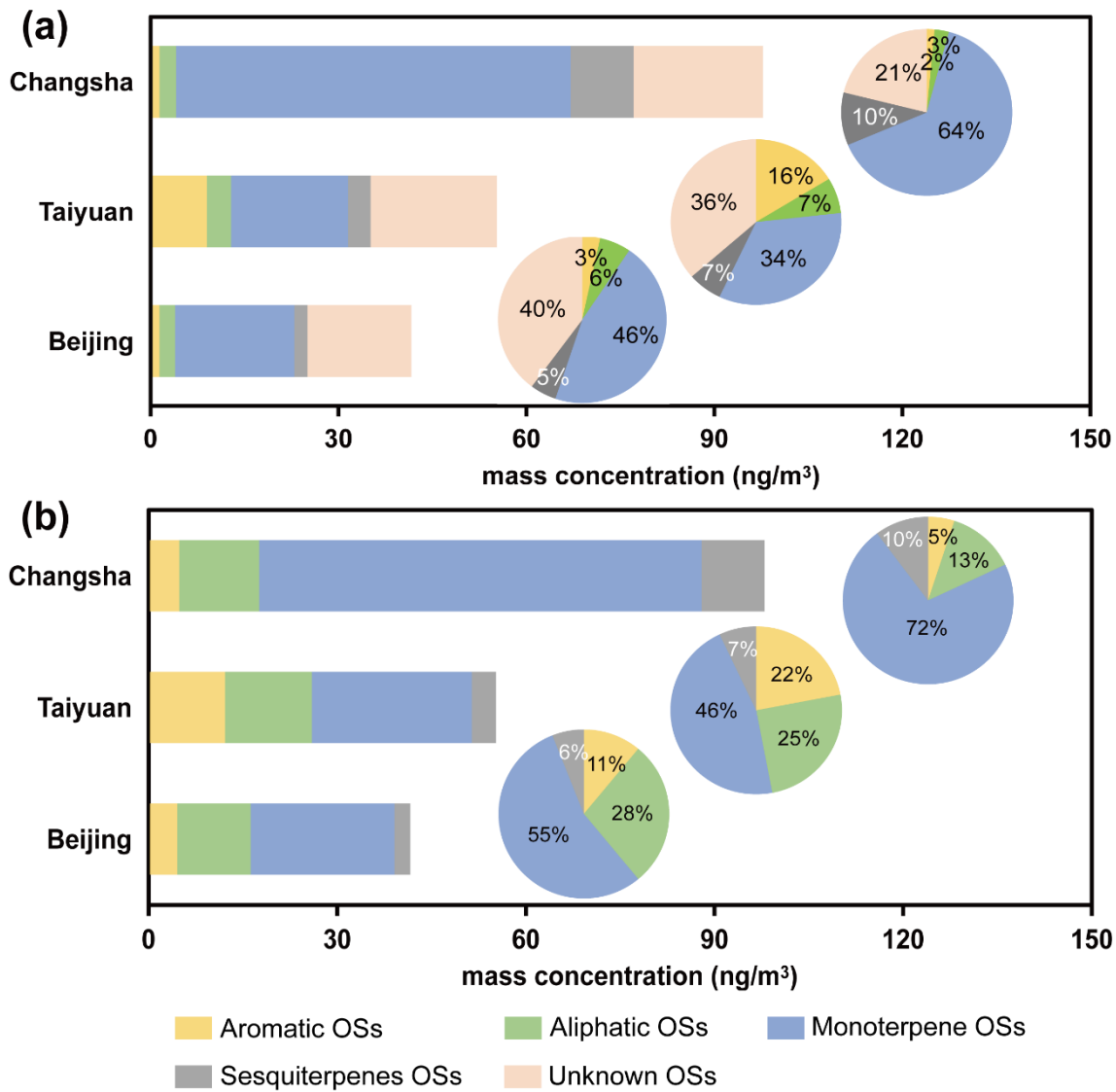
280 It is noteworthy that the single highest OS/OA ratio in Beijing was observed on December 31st
 281 under low RH. This phenomena highlights that ALWC, while a major driving factor of OS formation,

282 is not an exclusive control. Specifically, this day showed high atmospheric oxidative capacity and
283 aerosol acidity. We note that under such conditions, efficient acid-catalyzed heterogeneous reactions
284 of gas-phase oxidation products could drive substantial OS formation. The impact of ALWC,
285 atmospheric oxidative capacity, and aerosol pH on OS formation will be discussed in detail in Section
286 3.2.

287 Figures 2(a) and 2(b) shows the average mass concentrations and fractions of different OSs
288 categories across the three cities, based on classification approach based on OSs' elemental
289 composition and laboratory chamber-derived precursor–OS relationships and our precursor-based
290 PMF classification approach developed in this work, respectively (see Section 2.3 for details). As
291 displayed in Figure 2(b), Monoterpene OSs dominated detected OSs across all cities, contributing 55.2%
292 (Beijing), 46.8% (Taiyuan), and 72.3% (Changsha) to total OS, respectively. Biogenic-emitted
293 monoterpene is the precursor of Monoterpene OSs. However, monoterpene are primarily biogenic
294 precursors, their limited emissions during winter cannot fully explain the high mass fractions of
295 Monoterpene OSs. Recent studies have highlighted anthropogenic sources, particularly biomass
296 burning, as significant contributors to monoterpene (Wang et al., 2022a; Koss et al., 2018). The PM_{2.5}
297 source apportionment analysis (Text S2, Figure S6) confirmed that biomass burning substantially
298 contributed to PM_{2.5} across all cities. The highest total mass fractions of Monoterpene OSs in
299 Changsha are mainly attributed to the high RH (Table S6), which facilitates their formation via
300 heterogeneous reactions (Hettiyadura et al., 2017; Wang et al., 2018; Ding et al., 2016a; Ding et al.,
301 2016b; Li et al., 2020).

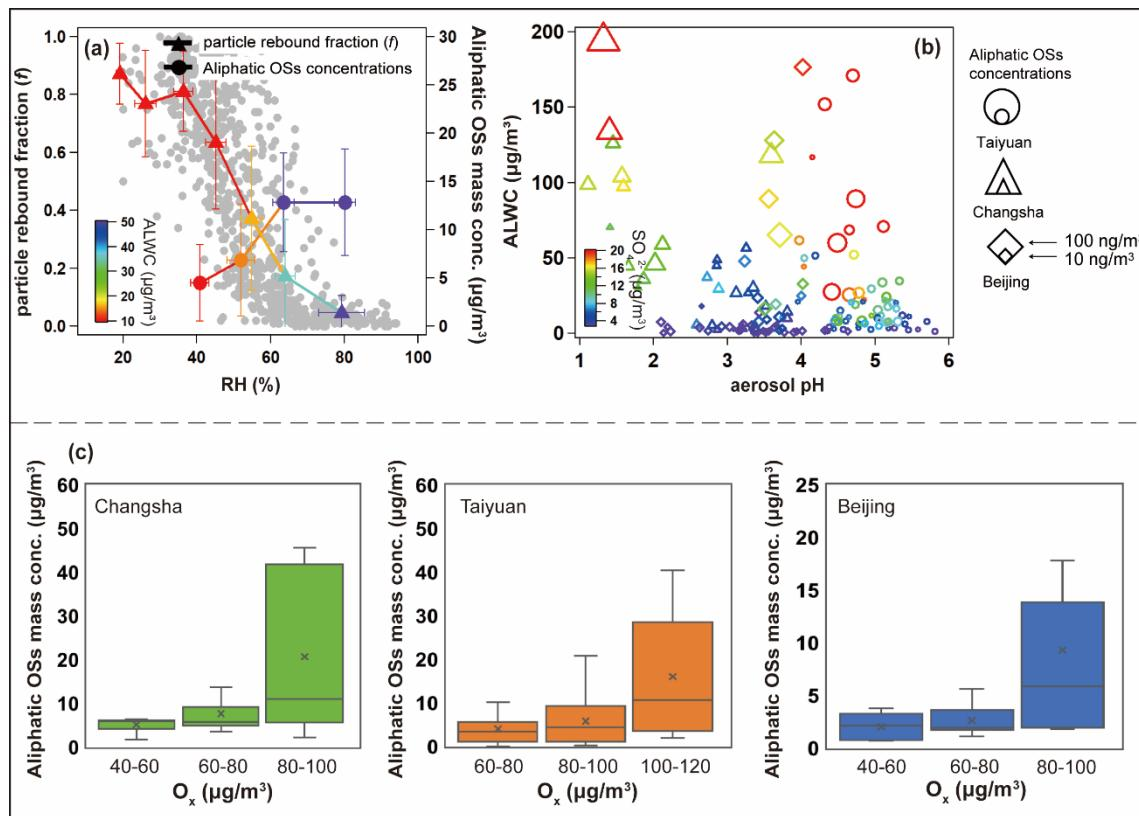
302 In Taiyuan, the total mass fractions of Aromatic OSs (21.2%) were significantly higher than those
303 in Beijing (10.7%) and Changsha (4.6%). Aromatic OSs primarily formed via aqueous-phase reactions
304 between S(IV) and aromatic VOCs (Huang et al., 2020). Taiyuan exhibited the highest sulfate mass
305 concentration among the three cities (Table S6), which promoted the formation of these species.
306 Additionally, transition metal ions—particularly Fe³⁺—catalyze aqueous-phase formation of Aromatic
307 OSs (Huang et al., 2020). High Fe mass concentration was observed in Taiyuan (0.79 ± 0.53 µg/m³),
308 further facilitated the formation of Aromatic OSs.

309 The highest total mass fractions of Aliphatic OSs were observed in Beijing (28.1%). Since vehicle
310 emissions, which is an important source of long-chain alkenes (He et al., 2022; Wang et al., 2021a;
311 Riva et al., 2016b; Tao et al., 2014; Tang et al., 2020), substantially contributed to PM_{2.5} in all cities
312 (Figure S6), the relative dominance of Aliphatic OSs in Beijing can be attributed to a comparative
313 reduction in the emissions of precursors for Monoterpene OSs and Aromatic OSs. Specifically, Beijing
314 exhibits lower emissions of monoterpene and aromatic VOCs precursors relative to Taiyuan and
315 Changsha, which results in a reduced contribution of Monoterpene and Aromatic OSs to the total OS
316 (see Figure 2(b)). Therefore, the relative mass fraction of Aliphatic OSs, which primarily derived from
317 between sulfate and photooxidation products of alkenes (Riva et al., 2016b), becomes more prominent
318 in Beijing. Additionally, low RH in Beijing further suppresses the aqueous-phase formation of
319 Monoterpene OSs, amplifying the relative importance of Aliphatic OSs.



335 60%) conditions.

336 In Changsha, where RH remains consistently high, Aliphatic OSs mass concentrations strongly
337 correlated with RH ($R = 0.78$). In Beijing and Taiyuan, correlations increased from low to medium
338 RH (Beijing: 0.53 to 0.82; Taiyuan: 0.38 to 0.77) but declined slightly at higher RH (Beijing: 0.82 to
339 0.69; Taiyuan: 0.77 to 0.72). The initial correlation rise reflects ALWC-enhanced sulfate-driven
340 heterogeneous OS formation (Wang et al., 2016b; Cheng et al., 2016b), while the decline at elevated
341 RH may due to the increase in ALWC dilutes the concentrations of precursors and intermediates of
342 Aliphatic OSs within the aqueous phase. Therefore, Aliphatic OSs formation were not further
343 promoted, exhibiting the non-linear response of their mass concentrations and ALWC.



344

345 **Figure 3** (a) The measured particle rebound fraction (f) and total mass concentrations of Aliphatic OSs
346 as a function of RH, the plots were colored by the calculated ALWC concentrations in Taiyuan, grey
347 dots indicate the mass concentrations of Aliphatic OSs; (b) the relationship between aerosol pH and
348 ALWC across three cities, the markers were colored by the inorganic sulfate mass concentrations, the
349 marker sizes represented the total mass concentrations of Aliphatic OSs; (c) the box plot of total mass
350 concentrations of Aliphatic OSs at different O_x concentration levels.

351 This threshold behavior aligns with aerosol phase transitions. Particle rebound fraction (f),
352 indicating phase state, was measured in Taiyuan using a three-arm impactor (Liu et al., 2017). As RH
353 exceeded 60%, f dropped below 0.2 (Figure 3(a)), signaling a transition from non-liquid to liquid
354 aerosol states. This transition at RH > 60% aligns with prior field (Liu et al., 2017; Liu et al., 2023;
355 Meng et al., 2024; Song et al., 2022) and modeling (Qiu et al., 2023) studies in Eastern China.
356 Correspondingly, Aliphatic OSs concentrations increased with RH below 60% but plateaued beyond
357 that despite further humidity rises. These findings underscore aerosol phase state as a critical factor:

358 initial liquid phase formation (RH < 60%) promotes heterogeneous OS formation (Ye et al., 2018),
359 whereas at higher RH, saturation of reactive interfaces limits further ALWC effects.

360 In addition, the increase in ALWC with rising RH altered aerosol pH (Figure 3(b)), which
361 inhibited OSs formation via acid-catalyzed reactions (Duporté et al., 2016). In Changsha, as aerosol
362 pH increased from approximately 1.0 to above 3.0, the average total mass concentrations of Aliphatic
363 OSs decreased significantly from 9.3 to 4.6 ng/m³ (Figure S8), with further declines as pH increased.
364 In Taiyuan, OS concentrations dropped from 12.2 to 6.8 ng/m³ as pH rose from below 4.5 to above
365 5.0. However, in Beijing, total mass concentrations of Aliphatic OSs remained stable within a narrow
366 pH range of 3.2–3.9. Elevated ALWC facilitates aqueous-phase radical chemistry that forms OSs via
367 non-acid pathways, which can dominate over pH-dependent processes (Rudziński et al., 2009; Wach
368 et al., 2019; Huang et al., 2019). Thus, pH-dependent suppression of Aliphatic OSs formation is
369 common across urban aerosol pH ranges, but less evident when pH varies narrowly.

370 Inorganic sulfate plays a crucial role in OS formation via sulfate esterification reactions (Xu et
371 al., 2024; Wang et al., 2020). We thus examined its effect on the formation of Aliphatic OSs. Figure
372 3(b) illustrates the relationships among ALWC, pH, inorganic sulfate mass concentration, and total
373 mass concentrations of Aliphatic OSs across all cities. A consistent positive correlation was observed,
374 consistent with previous field studies (Lin et al., 2022; Wang et al., 2023b; Le Breton et al., 2018;
375 Wang et al., 2018). This correlation was strongest when sulfate concentrations were below 20 µg/m³.
376 Below this threshold, total mass concentrations of Aliphatic OSs increased significantly with inorganic
377 sulfate, whereas above it, the correlation weakened. Additionally, inorganic sulfate mass concentration
378 showed a clear positive correlation with ALWC (Figure 3(b)), suggesting that ionic strength did not
379 increase linearly with sulfate mass. This likely reflects saturation effects in acid-mediated pathways,
380 driven by limitations in water activity and ionic strength (Wang et al., 2020). Overall, these results
381 highlight the nonlinear influence of inorganic sulfate on Aliphatic OSs formation.

382 Atmospheric oxidative capacity, represented by O_x (O_x = O₃ + NO₂) concentrations, typically
383 modulates OS formation via acid-catalyzed ring-opening reactions pathways. As shown in Figure 3(c),
384 total mass concentrations of Aliphatic OSs and NOSs exhibited significant increases with rising O_x
385 levels across all cities. Especially, total mass concentrations of Aliphatic OSs significantly increased
386 across all cities when O_x concentrations raised from 60–80 µg/m³ to > 80 µg/m³. As shown in Figure
387 S9, O₃ dominated the O_x composition during high-O_x episodes (> 80 µg/m³) across all cities. Previous
388 laboratory studies have suggested that enhanced atmospheric oxidation capacities promote the
389 oxidation of VOCs (Zhang et al., 2022; Wei et al., 2024), forming cyclic intermediates. We therefore
390 inferred that the increase in O_x facilitates the formation of cyclic intermediates derived from long-
391 chain alkenes. Subsequent acid-catalyzed and ring-opening reactions are important pathways of
392 heterogeneous OSs formation, including Aliphatic OSs (Eddingsaas et al., 2010; Iinuma et al., 2007;
393 Brüggemann et al., 2020).

394 It should be noted that though formation driving factors of Aliphatic OSs identified in this work,
395 including ALWC, inorganic sulfate, and O_x, are likely applicable in other urban environments sharing
396 similar winter conditions characterized by high anthropogenic emissions and moderate-to-high
397 humidity. However, their importance may differ in other cities with different atmospheric conditions,
398 like in summer with strong biogenic emissions, in regions with low aerosol acidity, or in arid cities
399 with persistently low RH.

400 **4 Conclusions and Implications**

401 In this study, we applied a NTA approach based on UHPLC-HRMS to investigate the molecular
402 composition of OS in PM_{2.5} samples from three cities. By integrating molecular composition data,
403 precursor-constrained PMF source apportionment, and OS-precursor correlation analysis, we
404 developed a comprehensive method for accurate classification of detected OSs, demonstrating
405 superior discrimination between Aliphatic OSs. Conventional classification methods rely on
406 laboratory chamber-derived precursor-OS relationships (Wang et al., 2019a), which provide limited
407 insight into the formation of Aliphatic OSs and tend to underestimate their mass fractions. The
408 abundant Aliphatic OSs detected in ambient PM_{2.5} suggest complex formation pathways, such as OH
409 oxidation of long-chain alkenes (Riva et al., 2016b) and heterogeneous reactions between SO₂ and
410 alkene in acidic conditions (Passananti et al., 2016), which remain incompletely understood in
411 laboratory studies. Our findings highlight the importance of emphasizing the formation of Aliphatic
412 OSs in urban atmospheres.

413 This study still faces several challenges. This work was conducted during the winter. OS
414 formation exhibits seasonal variability, particularly for pathways driven by biogenic VOCs emissions
415 and photochemical activity, which are generally enhanced in warmer months. Hence, the
416 underestimation of Aliphatic OSs, and their key formation factors determined in this work remain
417 valid insights for the winter period but may not fully represent annual OS behavior. In addition, our
418 field campaigns were conducted in three typical different Chinese cities, the effect of these driving
419 factors on the formation of Aliphatic OSs may not be applicable to other cities with different
420 atmospheric conditions. Future long-term observations in more cities are necessary to resolve the
421 complete annual cycle of OS composition, quantify the shifting contributions of anthropogenic versus
422 biogenic precursors, and understanding how key formation driving factors evolve with changing
423 atmospheric conditions.

424 For NTA, the use of surrogate standards for quantification OS mass concentration introduced
425 uncertainty, particularly due to the extraction efficiency of individual OSs species from quartz fiber
426 filters could not be determined. Although we have adopted standardized extraction protocol ensures
427 high comparability across our samples, absolute extraction recoveries may vary. In addition, this
428 approach depends on public molecular composition such as mzCloud and ChemSpider integrated
429 within the Compound Discoverer software, which contain limited entries for organosulfates. Reliance
430 on these databases for compound identification may therefore underestimate OS mass concentrations
431 in urban environments. For example, OSs identified here accounted for less than 1% of total OA mass,
432 whereas recent work (Ma et al., 2025) reported approximately 20% contributions.

433 OS may become increasingly significant in OA, particularly in coastal regions influenced by
434 oceanic dimethyl sulfate emissions (Brüggemann et al., 2020). Our future work will focus on
435 synthesizing OSs standards representing various precursors and establishing a dedicated fragmentation
436 database through multi-platform MS² validation to elucidate OS sources in more detail.

437 **Author Contributions**

438 Y.Q., J.W., and Z.W. designed this work. J.L., Y.Wei, C.L., J.Y., T.L., R.M., T.Z., W.F., J.Y., Z.F., Y.X.

439 and K.B. collected PM_{2.5} samples. Y.Q., J.W., T.Q., Y.B., and D.L. conducted UHPLC-HRMS
440 experiments. Y.Q., J.W., Z.G., and Y.Wang wrote this manuscript. Z.W., Y.Wang, and M.H. edited this
441 manuscript. All authors have read and agreed to submit this manuscript. Y.Q. and J.W. contributed
442 equally to this work.

443 **Funding**

444 This work is funded by the National Nature Science Foundation of China (Grants 22221004 and
445 22306059), This work was also supported by the Science and Technology Innovation Program of
446 Hunan Province (Grants 2024RC3106 and 2025AQ2001), and the Fundamental Research Funds
447 for the Central Universities (Grant 531118010830).

448 **Notes**

449 The authors declare that they have no conflict of interest.

450 **Acknowledgements**

451 Y.W would like to acknowledge financial support by the National Nature Science Foundation of
452 China (Grants 22221004 and 22306059), This work was also supported by the Science and
453 Technology Innovation Program of Hunan Province (Grants 2024RC3106 and 2025AQ2001),
454 and the Fundamental Research Funds for the Central Universities (Grant 531118010830).

455

456 **References**

457 Bateman, A. P., Belassein, H., Martin, S. T.: Impactor Apparatus for the Study of Particle Rebound:
458 Relative Humidity and Capillary Forces. *Aerosol Science and Technology*. 48, 42-52.
459 10.1080/02786826.2013.853866, 2014.

460 Brown, S. S., Dubé, W. P., Karamchandani, P., Yarwood, G., Peischl, J., Ryerson, T. B., Neuman, J. A.,
461 Nowak, J. B., Holloway, J. S., Washenfelder, R. A., Brock, C. A., Frost, G. J., Trainer, M., Parrish, D. D.,
462 Fehsenfeld, F. C., Ravishankara, A. R.: Effects of NO_x control and plume mixing on nighttime chemical
463 processing of plumes from coal-fired power plants. *Journal of Geophysical Research: Atmospheres*. 117.
464 <https://doi.org/10.1029/2011JD016954>, 2012.

465 Brüggemann, M., Xu, R., Tilgner, A., Kwong, K. C., Mutzel, A., Poon, H. Y., Otto, T., Schaefer, T.,
466 Poulain, L., Chan, M. N., Herrmann, H.: Organosulfates in Ambient Aerosol: State of Knowledge and
467 Future Research Directions on Formation, Abundance, Fate, and Importance. *Environmental Science &*
468 *Technology*. 54, 3767-3782. 10.1021/acs.est.9b06751, 2020.

469 Cai, D., Wang, X., Chen, J., Li, X.: Molecular Characterization of Organosulfates in Highly Polluted
470 Atmosphere Using Ultra-High-Resolution Mass Spectrometry. *Journal of Geophysical Research: Atmospheres*. 125, e2019JD032253. <https://doi.org/10.1029/2019JD032253>, 2020.

472 Cao, G., Zhao, X., Hu, D., Zhu, R., Ouyang, F.: Development and application of a quantification
473 method for water soluble organosulfates in atmospheric aerosols. *Environmental Pollution*. 225, 316-322.
474 <https://doi.org/10.1016/j.envpol.2017.01.086>, 2017.

475 Cheng, Y., Zheng, G., Wei, C., Mu, Q., Zheng, B., Wang, Z., Gao, M., Zhang, Q., He, K., Carmichael,
476 G., Pöschl, U., Su, H.: Reactive nitrogen chemistry in aerosol water as a source of sulfate during haze events
477 in China. *Science Advances*. 2, e1601530. 10.1126/sciadv.1601530, 2016a.

478 Cheng, Y., Zheng, G., Wei, C., Mu, Q., Zheng, B., Wang, Z., Gao, M., Zhang, Q., He, K., Carmichael,
479 G., Pöschl, U., Su, H.: Reactive nitrogen chemistry in aerosol water as a source of sulfate during haze events
480 in China. 2, e1601530. doi:10.1126/sciadv.1601530, 2016b.

481 Deng, Y., Inomata, S., Sato, K., Ramasamy, S., Morino, Y., Enami, S., Tanimoto, H.: Temperature and
482 acidity dependence of secondary organic aerosol formation from α -pinene ozonolysis with a compact
483 chamber system. *Atmos. Chem. Phys.* 21, 5983-6003. 10.5194/acp-21-5983-2021, 2021.

484 Ding, X., He, Q.-F., Shen, R.-Q., Yu, Q.-Q., Zhang, Y.-Q., Xin, J.-Y., Wen, T.-X., Wang, X.-M.: Spatial
485 and seasonal variations of isoprene secondary organic aerosol in China: Significant impact of biomass
486 burning during winter. *Scientific Reports*. 6, 20411. 10.1038/srep20411, 2016a.

487 Ding, X., Zhang, Y.-Q., He, Q.-F., Yu, Q.-Q., Shen, R.-Q., Zhang, Y., Zhang, Z., Lyu, S.-J., Hu, Q.-H.,
488 Wang, Y.-S., Li, L.-F., Song, W., Wang, X.-M.: Spatial and seasonal variations of secondary organic aerosol
489 from terpenoids over China. *Journal of Geophysical Research: Atmospheres*. 121, 14,661-614,678.
490 <https://doi.org/10.1002/2016JD025467>, 2016b.

491 Duporté, G., Flaud, P. M., Geneste, E., Augagneur, S., Pangui, E., Lamkaddam, H., Gratien, A.,
492 Doussin, J. F., Budzinski, H., Villenave, E., Perraudin, E.: Experimental Study of the Formation of

493 Organosulfates from α -Pinene Oxidation. Part I: Product Identification, Formation Mechanisms and Effect
494 of Relative Humidity. *The Journal of Physical Chemistry A.* 120, 7909-7923. 10.1021/acs.jpca.6b08504,
495 2016.

496 Duporté, G., Flaud, P. M., Kammer, J., Geneste, E., Augagneur, S., Pangui, E., Lamkaddam, H.,
497 Gratien, A., Doussin, J. F., Budzinski, H., Villenave, E., Perraquin, E.: Experimental Study of the Formation
498 of Organosulfates from α -Pinene Oxidation. 2. Time Evolution and Effect of Particle Acidity. *The Journal*
499 of *Physical Chemistry A.* 124, 409-421. 10.1021/acs.jpca.9b07156, 2020.

500 Eddingsaas, N. C., VanderVelde, D. G., Wennberg, P. O.: Kinetics and Products of the Acid-Catalyzed
501 Ring-Opening of Atmospherically Relevant Butyl Epoxy Alcohols. *The Journal of Physical Chemistry A.*
502 114, 8106-8113. 10.1021/jp103907c, 2010.

503 Edwards, P. M., Aikin, K. C., Dube, W. P., Fry, J. L., Gilman, J. B., de Gouw, J. A., Graus, M. G.,
504 Hanisco, T. F., Holloway, J., Hübner, G., Kaiser, J., Keutsch, F. N., Lerner, B. M., Neuman, J. A., Parrish,
505 D. D., Peischl, J., Pollack, I. B., Ravishankara, A. R., Roberts, J. M., Ryerson, T. B., Trainer, M., Veres, P.
506 R., Wolfe, G. M., Warneke, C., Brown, S. S.: Transition from high- to low-NO_x control of night-time
507 oxidation in the southeastern US. *Nature Geoscience.* 10, 490-495. 10.1038/ngeo2976, 2017.

508 Estillore, A. D., Hettiyadura, A. P. S., Qin, Z., Leckrone, E., Wombacher, B., Humphry, T., Stone, E.
509 A., Grassian, V. H.: Water Uptake and Hygroscopic Growth of Organosulfate Aerosol. *Environmental*
510 *Science & Technology.* 50, 4259-4268. 10.1021/acs.est.5b05014, 2016.

511 Fleming, L. T., Ali, N. N., Blair, S. L., Roveretto, M., George, C., Nizkorodov, S. A.: Formation of
512 Light-Absorbing Organosulfates during Evaporation of Secondary Organic Material Extracts in the
513 Presence of Sulfuric Acid. *ACS Earth and Space Chemistry.* 3, 947-957.
514 10.1021/acsearthspacechem.9b00036, 2019.

515 Fountoukis, C., Nenes, A.: ISORROPIA II: a computationally efficient thermodynamic equilibrium
516 model for K⁺; Ca²⁺; Mg²⁺; NH⁴⁺; Na⁺; SO₄²⁻; NO₃⁻; Cl⁻; H₂O aerosols. *Atmospheric Chemistry and*
517 *Physics.* 7, 4639-4659. 10.5194/acp-7-4639-2007, 2007.

518 Guenther, A., Karl, T., Harley, P., Wiedinmyer, C., Palmer, P. I., Geron, C.: Estimates of global
519 terrestrial isoprene emissions using MEGAN (Model of Emissions of Gases and Aerosols from Nature).
520 *Atmos. Chem. Phys.* 6, 3181-3210. 10.5194/acp-6-3181-2006, 2006.

521 Hansen, A. M. K., Hong, J., Raatikainen, T., Kristensen, K., Ylisirniö, A., Virtanen, A., Petäjä, T.,
522 Glasius, M., Prisle, N. L.: Hygroscopic properties and cloud condensation nuclei activation of limonene-
523 derived organosulfates and their mixtures with ammonium sulfate. *Atmos. Chem. Phys.* 15, 14071-14089.
524 10.5194/acp-15-14071-2015, 2015.

525 He, J., Li, L., Li, Y., Huang, M., Zhu, Y., Deng, S.: Synthesis, MS/MS characteristics and quantification
526 of six aromatic organosulfates in atmospheric PM_{2.5}. *Atmospheric Environment.* 290, 119361.
527 <https://doi.org/10.1016/j.atmosenv.2022.119361>, 2022.

528 Hettiyadura, A. P. S., Jayarathne, T., Baumann, K., Goldstein, A. H., de Gouw, J. A., Koss, A., Keutsch,
529 F. N., Skog, K., Stone, E. A.: Qualitative and quantitative analysis of atmospheric organosulfates in
530 Centreville, Alabama. *Atmospheric Chemistry and Physics.* 17, 1343-1359. 10.5194/acp-17-1343-2017,
531 2017.

532 Hoyle, C. R., Boy, M., Donahue, N. M., Fry, J. L., Glasius, M., Guenther, A., Hallar, A. G., Huff Hartz,
533 K., Petters, M. D., Petäjä, T., Rosenoern, T., Sullivan, A. P.: A review of the anthropogenic influence on
534 biogenic secondary organic aerosol. *Atmos. Chem. Phys.* 11, 321-343. 10.5194/acp-11-321-2011, 2011.

535 Huang, L., Cochran, R. E., Coddens, E. M., Grassian, V. H.: Formation of Organosulfur Compounds
536 through Transition Metal Ion-Catalyzed Aqueous Phase Reactions. *Environmental Science & Technology
537 Letters.* 5, 315-321. 10.1021/acs.estlett.8b00225, 2018a.

538 Huang, L., Coddens, E. M., Grassian, V. H.: Formation of Organosulfur Compounds from Aqueous
539 Phase Reactions of S(IV) with Methacrolein and Methyl Vinyl Ketone in the Presence of Transition Metal
540 Ions. *ACS Earth and Space Chemistry.* 3, 1749-1755. 10.1021/acsearthspacechem.9b00173, 2019.

541 Huang, L., Liu, T., Grassian, V. H.: Radical-Initiated Formation of Aromatic Organosulfates and
542 Sulfonates in the Aqueous Phase. *Environmental Science & Technology.* 54, 11857-11864.
543 10.1021/acs.est.0c05644, 2020.

544 Huang, L., Wang, Y., Zhao, Y., Hu, H., Yang, Y., Wang, Y., Yu, J.-Z., Chen, T., Cheng, Z., Li, C., Li,
545 Z., Xiao, H.: Biogenic and Anthropogenic Contributions to Atmospheric Organosulfates in a Typical
546 Megacity in Eastern China. *Journal of Geophysical Research: Atmospheres.* 128, e2023JD038848.
547 <https://doi.org/10.1029/2023JD038848>, 2023a.

548 Huang, L., Wang, Y., Zhao, Y., Hu, H., Yang, Y., Wang, Y., Yu, J.-Z., Chen, T., Cheng, Z., Li, C., Li,
549 Z., Xiao, H.: Biogenic and Anthropogenic Contributions to Atmospheric Organosulfates in a Typical
550 Megacity in Eastern China. 128, e2023JD038848. <https://doi.org/10.1029/2023JD038848>, 2023b.

551 Huang, R. J., Cao, J., Chen, Y., Yang, L., Shen, J., You, Q., Wang, K., Lin, C., Xu, W., Gao, B., Li, Y.,
552 Chen, Q., Hoffmann, T., O'Dowd, C. D., Bilde, M., Glasius, M.: Organosulfates in atmospheric aerosol:
553 synthesis and quantitative analysis of PM2.5 from Xi'an, northwestern China. *Atmos. Meas. Tech.* 11, 3447-
554 3456. 10.5194/amt-11-3447-2018, 2018b.

555 Iinuma, Y., Müller, C., Berndt, T., Böge, O., Claeys, M., Herrmann, H.: Evidence for the Existence of
556 Organosulfates from β -Pinene Ozonolysis in Ambient Secondary Organic Aerosol. *Environmental Science
557 & Technology.* 41, 6678-6683. 10.1021/es070938t, 2007.

558 Jiang, H., Cai, J., Feng, X., Chen, Y., Guo, H., Mo, Y., Tang, J., Chen, T., Li, J., Zhang, G.:
559 Organosulfur Compounds: A Non-Negligible Component Affecting the Light Absorption of Brown Carbon
560 During North China Haze Events. *Journal of Geophysical Research: Atmospheres.* 130, e2024JD042043.
561 <https://doi.org/10.1029/2024JD042043>, 2025.

562 Koss, A. R., Sekimoto, K., Gilman, J. B., Selimovic, V., Coggon, M. M., Zarzana, K. J., Yuan, B.,
563 Lerner, B. M., Brown, S. S., Jimenez, J. L., Krechmer, J., Roberts, J. M., Warneke, C., Yokelson, R. J., de
564 Gouw, J.: Non-methane organic gas emissions from biomass burning: identification, quantification, and
565 emission factors from PTR-ToF during the FIREX 2016 laboratory experiment. *Atmos. Chem. Phys.* 18,
566 3299-3319. 10.5194/acp-18-3299-2018, 2018.

567 Le Breton, M., Wang, Y., Hallquist, Å. M., Pathak, R. K., Zheng, J., Yang, Y., Shang, D., Glasius, M.,
568 Bannan, T. J., Liu, Q., Chan, C. K., Percival, C. J., Zhu, W., Lou, S., Topping, D., Wang, Y., Yu, J., Lu, K.,
569 Guo, S., Hu, M., Hallquist, M.: Online gas- and particle-phase measurements of organosulfates,
570 organosulfonates and nitrooxy organosulfates in Beijing utilizing a FIGAERO ToF-CIMS. *Atmos. Chem.*

571 Phys. 18, 10355-10371. 10.5194/acp-18-10355-2018, 2018.

572 Li, L., Yang, W., Xie, S., Wu, Y.: Estimations and uncertainty of biogenic volatile organic compound
573 emission inventory in China for 2008–2018. Science of The Total Environment. 733, 139301.
574 <https://doi.org/10.1016/j.scitotenv.2020.139301>, 2020.

575 Lin, P., Yu, J. Z., Engling, G., Kalberer, M.: Organosulfates in Humic-like Substance Fraction Isolated
576 from Aerosols at Seven Locations in East Asia: A Study by Ultra-High-Resolution Mass Spectrometry.
577 Environmental Science & Technology. 46, 13118-13127. 10.1021/es303570v, 2012.

578 Lin, Y., Han, Y., Li, G., Wang, Q., Zhang, X., Li, Z., Li, L., Prévôt, A. S. H., Cao, J.: Molecular
579 Characteristics of Atmospheric Organosulfates During Summer and Winter Seasons in Two Cities of
580 Southern and Northern China. Journal of Geophysical Research: Atmospheres. 127, e2022JD036672.
581 <https://doi.org/10.1029/2022JD036672>, 2022.

582 Liu, P., Ding, X., Li, B. X., Zhang, Y. Q., Bryant, D. J., Wang, X. M.: Quality assurance and quality
583 control of atmospheric organosulfates measured using hydrophilic interaction liquid chromatography
584 (HILIC). Atmos. Meas. Tech. 17, 3067-3079. 10.5194/amt-17-3067-2024, 2024.

585 Liu, Y., Wu, Z., Wang, Y., Xiao, Y., Gu, F., Zheng, J., Tan, T., Shang, D., Wu, Y., Zeng, L., Hu, M.,
586 Bateman, A. P., Martin, S. T.: Submicrometer Particles Are in the Liquid State during Heavy Haze Episodes
587 in the Urban Atmosphere of Beijing, China. Environ. Sci. Technol. Lett. 4, 427-432.
588 10.1021/acs.estlett.7b00352, 2017.

589 Liu, Y. C., Wu, Z. J., Qiu, Y. T., Tian, P., Liu, Q., Chen, Y., Song, M., Hu, M.: Enhanced Nitrate Fraction:
590 Enabling Urban Aerosol Particles to Remain in a Liquid State at Reduced Relative Humidity. Geophysical
591 Research Letters. 50, e2023GL105505. <https://doi.org/10.1029/2023GL105505>, 2023.

592 Lukács, H., Gelencsér, A., Hoffer, A., Kiss, G., Horváth, K., Hartyáni, Z.: Quantitative assessment of
593 organosulfates in size-segregated rural fine aerosol. Atmos. Chem. Phys. 9, 231-238. 10.5194/acp-9-231-
594 2009, 2009.

595 Ma, J., Ungeheuer, F., Zheng, F., Du, W., Wang, Y., Cai, J., Zhou, Y., Yan, C., Liu, Y., Kulmala, M.,
596 Daellenbach, K. R., Vogel, A. L.: Nontarget Screening Exhibits a Seasonal Cycle of PM2.5 Organic Aerosol
597 Composition in Beijing. Environmental Science & Technology. 56, 7017-7028. 10.1021/acs.est.1c06905,
598 2022.

599 Ma, J., Reininger, N., Zhao, C., Döbler, D., Rüdiger, J., Qiu, Y., Ungeheuer, F., Simon, M., D'Angelo,
600 L., Breuninger, A., David, J., Bai, Y., Li, Y., Xue, Y., Li, L., Wang, Y., Hildmann, S., Hoffmann, T., Liu, B.,
601 Niu, H., Wu, Z., Vogel, A. L.: Unveiling a large fraction of hidden organosulfates in ambient organic aerosol.
602 Nature Communications. 16, 4098. 10.1038/s41467-025-59420-y, 2025.

603 Meng, X., Wu, Z., Chen, J., Qiu, Y., Zong, T., Song, M., Lee, J., Hu, M.: Particle phase state and
604 aerosol liquid water greatly impact secondary aerosol formation: insights into phase transition and its role
605 in haze events. Atmospheric Chemistry and Physics. 24, 2399-2414. 10.5194/acp-24-2399-2024, 2024.

606 Mutzel, A., Poulaïn, L., Berndt, T., Iinuma, Y., Rodigast, M., Böge, O., Richters, S., Spindler, G., Sipilä,
607 M., Jokinen, T., Kulmala, M., Herrmann, H.: Highly Oxidized Multifunctional Organic Compounds
608 Observed in Tropospheric Particles: A Field and Laboratory Study. Environmental Science & Technology.

609 49, 7754-7761. 10.1021/acs.est.5b00885, 2015.

610 Ohno, P. E., Wang, J., Mahrt, F., Varelas, J. G., Aruffo, E., Ye, J., Qin, Y., Kiland, K. J., Bertram, A.
611 K., Thomson, R. J., Martin, S. T.: Gas-Particle Uptake and Hygroscopic Growth by Organosulfate Particles.
612 ACS Earth and Space Chemistry. 6, 2481-2490. 10.1021/acsearthspacechem.2c00195, 2022.

613 Passananti, M., Kong, L., Shang, J., Dupart, Y., Perrier, S., Chen, J., Donaldson, D. J., George, C.:
614 Organosulfate Formation through the Heterogeneous Reaction of Sulfur Dioxide with Unsaturated Fatty
615 Acids and Long-Chain Alkenes. Angewandte Chemie International Edition. 55, 10336-10339.
616 <https://doi.org/10.1002/anie.201605266>, 2016.

617 Qiu, Y., Liu, Y., Wu, Z., Wang, F., Meng, X., Zhang, Z., Man, R., Huang, D., Wang, H., Gao, Y., Huang,
618 C., Hu, M.: Predicting Atmospheric Particle Phase State Using an Explainable Machine Learning Approach
619 Based on Particle Rebound Measurements. Environmental Science & Technology. 57, 15055-15064.
620 10.1021/acs.est.3c05284, 2023.

621 Riva, M., Tomaz, S., Cui, T., Lin, Y.-H., Perraудин, E., Gold, A., Stone, E. A., Villenave, E., Surratt, J.
622 D.: Evidence for an Unrecognized Secondary Anthropogenic Source of Organosulfates and Sulfonates:
623 Gas-Phase Oxidation of Polycyclic Aromatic Hydrocarbons in the Presence of Sulfate Aerosol.
624 Environmental Science & Technology. 49, 6654-6664. 10.1021/acs.est.5b00836, 2015.

625 Riva, M., Budisulistiorini, S. H., Zhang, Z., Gold, A., Surratt, J. D.: Chemical characterization of
626 secondary organic aerosol constituents from isoprene ozonolysis in the presence of acidic aerosol.
627 Atmospheric Environment. 130, 5-13. <https://doi.org/10.1016/j.atmosenv.2015.06.027>, 2016a.

628 Riva, M., Da Silva Barbosa, T., Lin, Y. H., Stone, E. A., Gold, A., Surratt, J. D.: Chemical
629 characterization of organosulfates in secondary organic aerosol derived from the photooxidation of alkanes.
630 Atmospheric Chemistry and Physics. 16, 11001-11018. 10.5194/acp-16-11001-2016, 2016b.

631 Riva, M., Da Silva Barbosa, T., Lin, Y. H., Stone, E. A., Gold, A., Surratt, J. D.: Chemical
632 characterization of organosulfates in secondary organic aerosol derived from the photooxidation of alkanes.
633 Atmos. Chem. Phys. 16, 11001-11018. 10.5194/acp-16-11001-2016, 2016c.

634 Riva, M., Chen, Y., Zhang, Y., Lei, Z., Olson, N. E., Boyer, H. C., Narayan, S., Yee, L. D., Green, H.
635 S., Cui, T., Zhang, Z., Baumann, K., Fort, M., Edgerton, E., Budisulistiorini, S. H., Rose, C. A., Ribeiro, I.
636 O., e Oliveira, R. L., dos Santos, E. O., Machado, C. M. D., Szopa, S., Zhao, Y., Alves, E. G., de Sá, S. S.,
637 Hu, W., Knipping, E. M., Shaw, S. L., Duvoisin Junior, S., de Souza, R. A. F., Palm, B. B., Jimenez, J.-L.,
638 Glasius, M., Goldstein, A. H., Pye, H. O. T., Gold, A., Turpin, B. J., Vizuete, W., Martin, S. T., Thornton, J.
639 A., Dutcher, C. S., Ault, A. P., Surratt, J. D.: Increasing Isoprene Epoxydiol-to-Inorganic Sulfate Aerosol
640 Ratio Results in Extensive Conversion of Inorganic Sulfate to Organosulfur Forms: Implications for
641 Aerosol Physicochemical Properties. Environmental Science & Technology. 53, 8682-8694.
642 10.1021/acs.est.9b01019, 2019.

643 Rudziński, K. J., Gmachowski, L., Kuznietsova, I.: Reactions of isoprene and sulphony radical-anions
644 – a possible source of atmospheric organosulphites and organosulphates. Atmos. Chem. Phys. 9, 2129-2140.
645 10.5194/acp-9-2129-2009, 2009.

646 Sakulyanontvittaya, T., Guenther, A., Helmig, D., Milford, J., Wiedinmyer, C.: Secondary Organic
647 Aerosol from Sesquiterpene and Monoterpene Emissions in the United States. Environmental Science &

648 Technology. 42, 8784-8790. 10.1021/es800817r, 2008.

649 Song, M., Jeong, R., Kim, D., Qiu, Y., Meng, X., Wu, Z., Zuend, A., Ha, Y., Kim, C., Kim, H., Gaikwad,
650 S., Jang, K. S., Lee, J. Y., Ahn, J.: Comparison of Phase States of PM2.5 over Megacities, Seoul and Beijing,
651 and Their Implications on Particle Size Distribution. Environmental Science and Technology. 56, 17581-
652 17590. 10.1021/acs.est.2c06377, 2022.

653 Staudt, S., Kundu, S., Lehmler, H.-J., He, X., Cui, T., Lin, Y.-H., Kristensen, K., Glasius, M., Zhang,
654 X., Weber, R. J., Surratt, J. D., Stone, E. A.: Aromatic organosulfates in atmospheric aerosols: Synthesis,
655 characterization, and abundance. Atmospheric Environment. 94, 366-373.
656 <https://doi.org/10.1016/j.atmosenv.2014.05.049>, 2014.

657 Surratt, J. D., Gómez-González, Y., Chan, A. W. H., Vermeylen, R., Shahgholi, M., Kleindienst, T. E.,
658 Edney, E. O., Offenberg, J. H., Lewandowski, M., Jaoui, M., Maenhaut, W., Claeys, M., Flagan, R. C.,
659 Seinfeld, J. H.: Organosulfate Formation in Biogenic Secondary Organic Aerosol. The Journal of Physical
660 Chemistry A. 112, 8345-8378. 10.1021/jp802310p, 2008.

661 Tang, J., Li, J., Su, T., Han, Y., Mo, Y., Jiang, H., Cui, M., Jiang, B., Chen, Y., Tang, J., Song, J., Peng,
662 P., Zhang, G.: Molecular compositions and optical properties of dissolved brown carbon in biomass burning,
663 coal combustion, and vehicle emission aerosols illuminated by excitation–emission matrix spectroscopy
664 and Fourier transform ion cyclotron resonance mass spectrometry analysis. Atmos. Chem. Phys. 20, 2513-
665 2532. 10.5194/acp-20-2513-2020, 2020.

666 Tao, S., Lu, X., Levac, N., Bateman, A. P., Nguyen, T. B., Bones, D. L., Nizkorodov, S. A., Laskin, J.,
667 Laskin, A., Yang, X.: Molecular Characterization of Organosulfates in Organic Aerosols from Shanghai and
668 Los Angeles Urban Areas by Nanospray-Desorption Electrospray Ionization High-Resolution Mass
669 Spectrometry. Environmental Science & Technology. 48, 10993-11001. 10.1021/es5024674, 2014.

670 Tolocka, M. P., Turpin, B.: Contribution of Organosulfur Compounds to Organic Aerosol Mass.
671 Environmental Science & Technology. 46, 7978-7983. 10.1021/es300651v, 2012.

672 Wach, P., Spólnik, G., Rudziński, K. J., Skotak, K., Claeys, M., Danikiewicz, W., Szmigielski, R.:
673 Radical oxidation of methyl vinyl ketone and methacrolein in aqueous droplets: Characterization of
674 organosulfates and atmospheric implications. Chemosphere. 214, 1-9.
675 <https://doi.org/10.1016/j.chemosphere.2018.09.026>, 2019.

676 Wang, G., Zhang, R., Gomez, M. E., Yang, L., Levy Zamora, M., Hu, M., Lin, Y., Peng, J., Guo, S.,
677 Meng, J., Li, J., Cheng, C., Hu, T., Ren, Y., Wang, Y., Gao, J., Cao, J., An, Z., Zhou, W., Li, G., Wang, J.,
678 Tian, P., Marrero-Ortiz, W., Secrest, J., Du, Z., Zheng, J., Shang, D., Zeng, L., Shao, M., Wang, W., Huang,
679 Y., Wang, Y., Zhu, Y., Li, Y., Hu, J., Pan, B., Cai, L., Cheng, Y., Ji, Y., Zhang, F., Rosenfeld, D., Liss, P. S.,
680 Duce, R. A., Kolb, C. E., Molina, M. J.: Persistent sulfate formation from London Fog to Chinese haze.
681 Proceedings of the National Academy of Sciences. 113, 13630-13635. 10.1073/pnas.1616540113, 2016a.

682 Wang, G., Zhang, R., Gomez, M. E., Yang, L., Levy Zamora, M., Hu, M., Lin, Y., Peng, J., Guo, S.,
683 Meng, J., Li, J., Cheng, C., Hu, T., Ren, Y., Wang, Y., Gao, J., Cao, J., An, Z., Zhou, W., Li, G., Wang, J.,
684 Tian, P., Marrero-Ortiz, W., Secrest, J., Du, Z., Zheng, J., Shang, D., Zeng, L., Shao, M., Wang, W., Huang,
685 Y., Wang, Y., Zhu, Y., Li, Y., Hu, J., Pan, B., Cai, L., Cheng, Y., Ji, Y., Zhang, F., Rosenfeld, D., Liss, P. S.,
686 Duce, R. A., Kolb, C. E., Molina, M. J.: Persistent sulfate formation from London Fog to Chinese haze.

687 113, 13630-13635. doi:10.1073/pnas.1616540113, 2016b.

688 Wang, H., Ma, X., Tan, Z., Wang, H., Chen, X., Chen, S., Gao, Y., Liu, Y., Liu, Y., Yang, X., Yuan, B.,
689 Zeng, L., Huang, C., Lu, K., Zhang, Y.: Anthropogenic monoterpenes aggravating ozone pollution. National
690 Science Review. 9, nwac103. 10.1093/nsr/nwac103, 2022a.

691 Wang, K., Zhang, Y., Huang, R.-J., Wang, M., Ni, H., Kampf, C. J., Cheng, Y., Bilde, M., Glasius, M.,
692 Hoffmann, T.: Molecular Characterization and Source Identification of Atmospheric Particulate
693 Organosulfates Using Ultrahigh Resolution Mass Spectrometry. Environmental Science & Technology. 53,
694 6192-6202. 10.1021/acs.est.9b02628, 2019a.

695 Wang, Y., Ren, J., Huang, X. H. H., Tong, R., Yu, J. Z.: Synthesis of Four Monoterpene-Derived
696 Organosulfates and Their Quantification in Atmospheric Aerosol Samples. Environmental Science &
697 Technology. 51, 6791-6801. 10.1021/acs.est.7b01179, 2017.

698 Wang, Y., Hu, M., Guo, S., Wang, Y., Zheng, J., Yang, Y., Zhu, W., Tang, R., Li, X., Liu, Y., Le Breton,
699 M., Du, Z., Shang, D., Wu, Y., Wu, Z., Song, Y., Lou, S., Hallquist, M., Yu, J.: The secondary formation of
700 organosulfates under interactions between biogenic emissions and anthropogenic pollutants in summer in
701 Beijing. Atmospheric Chemistry and Physics. 18, 10693-10713. 10.5194/acp-18-10693-2018, 2018.

702 Wang, Y., Ma, Y., Li, X., Kuang, B. Y., Huang, C., Tong, R., Yu, J. Z.: Monoterpene and Sesquiterpene
703 α -Hydroxy Organosulfates: Synthesis, MS/MS Characteristics, and Ambient Presence. Environmental
704 Science & Technology. 53, 12278-12290. 10.1021/acs.est.9b04703, 2019b.

705 Wang, Y., Hu, M., Wang, Y.-C., Li, X., Fang, X., Tang, R., Lu, S., Wu, Y., Guo, S., Wu, Z., Hallquist,
706 M., Yu, J. Z.: Comparative Study of Particulate Organosulfates in Contrasting Atmospheric Environments:
707 Field Evidence for the Significant Influence of Anthropogenic Sulfate and NOx. Environmental Science &
708 Technology Letters. 7, 787-794. 10.1021/acs.estlett.0c00550, 2020.

709 Wang, Y., Zhao, Y., Wang, Y., Yu, J. Z., Shao, J., Liu, P., Zhu, W., Cheng, Z., Li, Z., Yan, N., Xiao, H.:
710 Organosulfates in atmospheric aerosols in Shanghai, China: seasonal and interannual variability, origin, and
711 formation mechanisms. Atmos. Chem. Phys. 21, 2959-2980. 10.5194/acp-21-2959-2021, 2021a.

712 Wang, Y., Zhao, Y., Wang, Y., Yu, J. Z., Shao, J., Liu, P., Zhu, W., Cheng, Z., Li, Z., Yan, N., Xiao, H.:
713 Organosulfates in atmospheric aerosols in Shanghai, China: seasonal and interannual variability, origin, and
714 formation mechanisms. Atmospheric Chemistry and Physics. 21, 2959-2980. 10.5194/acp-21-2959-2021,
715 2021b.

716 Wang, Y., Ma, Y., Kuang, B., Lin, P., Liang, Y., Huang, C., Yu, J. Z.: Abundance of organosulfates
717 derived from biogenic volatile organic compounds: Seasonal and spatial contrasts at four sites in China.
718 Science of The Total Environment. 806, 151275. <https://doi.org/10.1016/j.scitotenv.2021.151275>, 2022b.

719 Wang, Y., Feng, Z., Yuan, Q., Shang, D., Fang, Y., Guo, S., Wu, Z., Zhang, C., Gao, Y., Yao, X., Gao,
720 H., Hu, M.: Environmental factors driving the formation of water-soluble organic aerosols: A comparative
721 study under contrasting atmospheric conditions. Science of The Total Environment. 866, 161364.
722 <https://doi.org/10.1016/j.scitotenv.2022.161364>, 2023a.

723 Wang, Y., Liang, S., Le Breton, M., Wang, Q. Q., Liu, Q., Ho, C. H., Kuang, B. Y., Wu, C., Hallquist,
724 M., Tong, R., Yu, J. Z.: Field observations of C2 and C3 organosulfates and insights into their formation

725 mechanisms at a suburban site in Hong Kong. *Science of The Total Environment*. 904, 166851.
726 <https://doi.org/10.1016/j.scitotenv.2023.166851>, 2023b.

727 Wei, L., Liu, R., Liao, C., Ouyang, S., Wu, Y., Jiang, B., Chen, D., Zhang, T., Guo, Y., Liu, S. C.: An
728 observation-based analysis of atmospheric oxidation capacity in Guangdong, China. *Atmospheric*
729 *Environment*. 318, 120260. <https://doi.org/10.1016/j.atmosenv.2023.120260>, 2024.

730 Wu, Z., Wang, Y., Tan, T., Zhu, Y., Li, M., Shang, D., Wang, H., Lu, K., Guo, S., Zeng, L., Zhang, Y.:
731 Aerosol Liquid Water Driven by Anthropogenic Inorganic Salts: Implying Its Key Role in Haze Formation
732 over the North China Plain. *Environmental Science & Technology Letters*. 5, 160-166.
733 10.1021/acs.estlett.8b00021, 2018.

734 Xu, L., Tsона, N. T., Du, L.: Relative Humidity Changes the Role of SO₂ in Biogenic Secondary
735 Organic Aerosol Formation. *The Journal of Physical Chemistry Letters*. 12, 7365-7372.
736 10.1021/acs.jpclett.1c01550, 2021a.

737 Xu, L., Yang, Z., Tsона, N. T., Wang, X., George, C., Du, L.: Anthropogenic–Biogenic Interactions at
738 Night: Enhanced Formation of Secondary Aerosols and Particulate Nitrogen- and Sulfur-Containing
739 Organics from β -Pinene Oxidation. *Environmental Science & Technology*. 55, 7794-7807.
740 10.1021/acs.est.0c07879, 2021b.

741 Xu, R., Chen, Y., Ng, S. I. M., Zhang, Z., Gold, A., Turpin, B. J., Ault, A. P., Surratt, J. D., Chan, M.
742 N.: Formation of Inorganic Sulfate and Volatile Nonsulfated Products from Heterogeneous Hydroxyl
743 Radical Oxidation of 2-Methyltetrol Sulfate Aerosols: Mechanisms and Atmospheric Implications.
744 *Environmental Science & Technology Letters*. 11, 968-974. 10.1021/acs.estlett.4c00451, 2024.

745 Yang, T., Xu, Y., Ye, Q., Ma, Y. J., Wang, Y. C., Yu, J. Z., Duan, Y. S., Li, C. X., Xiao, H. W., Li, Z. Y.,
746 Zhao, Y., Xiao, H. Y.: Spatial and diurnal variations of aerosol organosulfates in summertime Shanghai,
747 China: potential influence of photochemical processes and anthropogenic sulfate pollution. *Atmos. Chem.*
748 *Phys.* 23, 13433-13450. 10.5194/acp-23-13433-2023, 2023.

749 Yang, T., Xu, Y., Ma, Y.-J., Wang, Y.-C., Yu, J. Z., Sun, Q.-B., Xiao, H.-W., Xiao, H.-Y., Liu, C.-Q.:
750 Field Evidence for Constraints of Nearly Dry and Weakly Acidic Aerosol Conditions on the Formation of
751 Organosulfates. *Environmental Science & Technology Letters*. 11, 981-987. 10.1021/acs.estlett.4c00522,
752 2024.

753 Yassine, M. M., Harir, M., Dabek-Zlotorzynska, E., Schmitt-Kopplin, P.: Structural characterization
754 of organic aerosol using Fourier transform ion cyclotron resonance mass spectrometry: Aromaticity
755 equivalent approach. *Rapid Communications in Mass Spectrometry*. 28, 2445-2454.
756 <https://doi.org/10.1002/rcm.7038>, 2014.

757 Ye, C., Lu, K., Song, H., Mu, Y., Chen, J., Zhang, Y.: A critical review of sulfate aerosol formation
758 mechanisms during winter polluted periods. *Journal of Environmental Sciences*. 123, 387-399.
759 <https://doi.org/10.1016/j.jes.2022.07.011>, 2023.

760 Ye, J., Abbatt, J. P. D., Chan, A. W. H.: Novel pathway of SO₂ oxidation in the atmosphere: reactions
761 with monoterpene ozonolysis intermediates and secondary organic aerosol. *Atmos. Chem. Phys.* 18, 5549-
762 5565. 10.5194/acp-18-5549-2018, 2018.

763 Zhang, Y., Chen, Y., Lei, Z., Olson, N. E., Riva, M., Koss, A. R., Zhang, Z., Gold, A., Jayne, J. T.,
764 Worsnop, D. R., Onasch, T. B., Kroll, J. H., Turpin, B. J., Ault, A. P., Surratt, J. D.: Joint Impacts of Acidity
765 and Viscosity on the Formation of Secondary Organic Aerosol from Isoprene Epoxydiols (IEPOX) in Phase
766 Separated Particles. *ACS Earth and Space Chemistry*. 3, 2646-2658. 10.1021/acsearthspacechem.9b00209,
767 2019.

768 Zhang, Z., Jiang, J., Lu, B., Meng, X., Herrmann, H., Chen, J., Li, X.: Attributing Increases in Ozone
769 to Accelerated Oxidation of Volatile Organic Compounds at Reduced Nitrogen Oxides Concentrations.
770 *PNAS Nexus*. 1, pgac266. 10.1093/pnasnexus/pgac266, 2022.

771 Zhao, D., Schmitt, S. H., Wang, M., Acir, I. H., Tillmann, R., Tan, Z., Novelli, A., Fuchs, H., Pullinen,
772 I., Wegener, R., Rohrer, F., Wildt, J., Kiendler-Scharr, A., Wahner, A., Mentel, T. F.: Effects of NO_x and
773 SO₂ on the secondary organic aerosol formation from photooxidation of α -pinene and limonene. *Atmos.*
774 *Chem. Phys.* 18, 1611-1628. 10.5194/acp-18-1611-2018, 2018.

775 Zheng, B., Zhang, Q., Zhang, Y., He, K. B., Wang, K., Zheng, G. J., Duan, F. K., Ma, Y. L., Kimoto,
776 T.: Heterogeneous chemistry: a mechanism missing in current models to explain secondary inorganic
777 aerosol formation during the January 2013 haze episode in North China. *Atmos. Chem. Phys.* 15, 2031-
778 2049. 10.5194/acp-15-2031-2015, 2015.

779